



Research Article

Magnetohydrodynamic natural convection of complex fluids in a square porous cavity: A numerical simulation

S. VIGNESHWARI¹, B. REDDAPPA^{1,*}, B. RUSHI KUMAR²

¹Department of Mathematics, Kalasalingam Academy of Research and Education (Deemed to be University), School of Advanced Sciences, Tamil Nadu, 626126, India

²Department of Mathematics, Vellore Institute of Technology, School of Advanced Sciences, Tamil Nadu, 632014, India

ARTICLE INFO

Article history

Received: 12 April 2024

Revised: 20 September 2024

Accepted: 21 September 2024

Keywords:

Galerkin Finite Element Method; Jeffrey Fluid; Magnetohydrodynamics; Natural Convection; Porous Cavity

ABSTRACT

The primary objective of the present study is to investigate the influence of magnetohydrodynamic (MHD) flow and heat transfer behavior of Jeffrey fluid under natural convection within a square cavity filled with a permeable matrix. This investigation is significant because enhancing heat transfer capabilities in systems such as nuclear reactor cooling is crucial for ensuring efficient thermal management. The cavity is configured with cold vertical walls, an adiabatic top surface, and a heated bottom surface, while a constant vertical magnetic field is applied at the left wall. The momentum transfer in the permeable matrix is modelled using the Darcy–Forchheimer approach, and the Galerkin finite element method (GFEM) is employed within COMSOL Multiphysics 6.1 to solve the governing equations. The study examines a range of Rayleigh numbers ($10^3 \leq Ra \leq 10^6$), Darcy numbers ($10^{-5} \leq Da \leq 10^{-3}$), and Hartmann numbers ($10 \leq Ha \leq 40$), providing a detailed analysis of the Nusselt number, velocity distribution, isocontours, isotherms, temperature profiles, and stream functions. Key findings of the study reveal that as the Hartmann number increases, the velocity distribution exhibits a monotonic rise which indicating the strong influence of the magnetic field on flow dynamics. Numerical results of the study demonstrate that with an increase in the Hartmann number (Ha) from 10 to 40, the average Nusselt number on the hot wall decreases from 13.645 to 12.380 at a Rayleigh number (Ra) of 10^6 indicate a reduction in heat transfer efficiency due to the damping effect of the magnetic field. For lower Rayleigh numbers ($Ra = 10^3$) the Nusselt number remains nearly constant around 5.728 across varying Hartmann numbers which shows that the magnetic field's impact is less significant under weaker convective conditions. The results of the study show a high degree of consistency with previous studies, demonstrating the robustness of the numerical approach. This work advances the understanding of MHD natural convection with Jeffrey fluids by offering specific, quantitative insights that go beyond previous literature, particularly in the context of optimizing heat transfer in engineering applications. The novelty of present findings are particularly relevant to geophysical applications, such as modeling the movement of magma in volcanic cavities, as well as industrial processes like polymer mixing.

Cite this article as: Vigneshwari S, Reddappa B, Rushi Kumar B. Magnetohydrodynamic natural convection of complex fluids in a square porous cavity: A numerical simulation. J Ther Eng 2025;11(3):780–799.

*Corresponding author.

*E-mail address: drbreddappa@gmail.com

This paper was recommended for publication in revised form by Editor-in-Chief Ahmet Selim Dalkılıç



INTRODUCTION

Heat may move from one fluid to another or from one surface to a fluid that flows over it via bulk flow or mixed molecule diffusion. Convection is the term for this action. The heat transport in convection was calculated via Newton's law of cooling [1, 2]. Since natural convection heat transfer is frequently employed in engineering systems, much research has been conducted on this topic. Natural convection is a thermofluidic process that moves heat across temperature gradients because of buoyancy. The physics of natural convection and computer analysis are fundamental to many industries, including the cooling of heat-generating components, solar energy gathering, heat exchanger design, metrology, building insulation, crystal formation, and the nuclear industry [3, 4].

The phenomenon of heat transmission has numerous applications in science, engineering, and industry, making it a valuable research topic. As a scenario, heat is dissipated by electronic equipment, which in turn drives the textile industry, building cooling and heating systems, automobiles, phase-change materials, etc. Due to the aforementioned uses, academics are now interested in studying heat transport mechanisms through theoretical and experimental investigations, which will save time and money. The emphasis of research has shifted within this paradigm to effective means of heat transfer across Newtonian and non-Newtonian fluids in a range of geometries [2, 5–10]. Newtonian fluids are no longer regarded as appropriate, as non-Newtonian fluids are utilized in technical and engineering applications. These fluids are employed in a wide range of technological and industrial processes, such as the extraction of petroleum products from crude oil, food processing, biotechnology, and drilling activities [11]. This has increased scientists' curiosity about the intricacy of non-Newtonian fluids. Stress causes a variety of materials to vary in viscosity, including blood, honey, ketchup, egg whites, mayonnaise, paints, slurries, and melting chocolate. These materials also behave in a non-Newtonian manner. Since the flow behavior of non-Newtonian fluids is complicated, their characteristics cannot be sufficiently represented by a single model. Researchers have sometimes created a variety of flow models, the Maxwell model [12] including the power-law model [13], the Jeffrey model [14, 15], and other viscoplastic flow models, in an effort to better understand the process behind the movement of these fluids. A thorough analysis of fluid flow and heat pattern migration is necessary in both simple and complicated systems.

Numerous scholars have used theoretical analysis and numerical experimentation to study natural convection in a variety of cavities. Raisi [16] investigated non-Newtonian fluid flow inside a square cavity under natural convection with a heat source at the bottom of the square enclosure. The findings of the study were that the average Nusselt number increases for shear-thinning fluids and decreases for shear-thickening fluids compared with Newtonian fluids. In addition to magnetic flux, Dimitrienko [17] reported

that the angle of inclination has a significant effect on flow and heat transmission. The digital investigation of free convection caused by a thermally driven flow in the presence of an angled magnetic flux, taking into account the effects of Rayleigh Ra , Hartmann Ha , and flux angles, was conducted by Liao et al. [18]. Their findings revealed that the direction of the applied magnetic flux had a significant effect on the streamlines and isotherms. Additionally, as the Hartmann number increased and the applied magnetic field became stronger, the mean Nusselt Nu and maximum streamline function decreased. Laminar magnetohydrodynamic free convection of a non-Newtonian fluid in a square box with a constant magnetic flux in several directions.

Because of their many technological uses, heat transfer and other non-Newtonian fluid flows have attracted increasing research attention. The shear stress-strain relationships for these fluids are very different from those of the typical Newtonian model. Several mathematical models have been proposed to explain the various properties of non-Newtonian fluids. Numerous sectors, such as solar energy, aviation, and the military, employ holes extensively. This type of heat exchanger, which employs non-Newtonian fluids, has been studied by several academics [19–24]. Owing to their widespread usage, non-Newtonian fluids have been the subject of studies on heat transfer in cavities filled with them [25–28].

Jeffrey fluid flow has numerous applications in numerous technical domains. Jeffrey fluid is extensively used in the polymer industry and in industrial fluids, including paint, paper, ketchup, and toothpaste. The magneto hydrodynamics (MHD) flow study views the fluid as electrically conducting, in contrast to conventional hydrodynamic flow. Moreover, it is not magnetic; rather, the item itself is not affected by electric currents; rather, the magnetic field is. A few current research endeavors pertaining to MHD include the fields of aerodynamics, flow management, metal forming, communications, high-speed aerodynamics, cooling nuclear reactors, plasma containment, propulsion and power generation, and electrical component transmission lines. A wide range of technical fields heavily depend on the usage of MHD phenomena, such as plasma research [29], boundary layer drag reduction [30], unswerving numerical simulations [31] medical science [32, 33], and seawater propulsion [34]. The instinct system of cilia motion has been deliberated specifically using the MHD flow of the Jeffrey flow model, metal extrusion processes, metallurgical material processing, chemical engineering flow control, oscillating current [35] and peristalsis flow [36–38]. Numerous industrial processes, including material production, continuous strip and filament cooling, and the distillation of molten metals and nonmetallic enclosures, rely heavily on a uniform magnetic field. A few MHD Jeffrey flow investigations with various geometries are available [39–44].”

Magnetohydrodynamic (MHD) flows have garnered significant interest due to their wide-ranging applications

in engineering and natural processes. While MHD effects on Newtonian fluids have been extensively studied, there is a noticeable gap in the literature regarding non-Newtonian fluids, particularly within porous media under natural convection conditions. This gap is significant given the relevance of non-Newtonian fluids, such as Jeffrey fluids, in modelling complex scenarios like magma movement in volcanic cavities and industrial processes involving polymer mixing. Previous research has focused primarily on simplified conditions that do not capture the intricacies of real-world applications, leaving the interaction between MHD and non-Newtonian fluids underexplored. To address this research gap, the present study investigates the effects of MHD on Jeffrey fluids within a porous square cavity. Utilizing COMSOL Multiphysics 6.1, the study solves the intricate, nonlinear governing equations through the Galerkin finite element method (GFEM). The analysis is extended to other non-Newtonian fluids, including Casson and Carreau fluids, and explores the impact of varying thermal and magnetic boundary conditions, as well as time-varying and spatially varying magnetic fields. This research enhances the understanding of complex interactions between fluid rheology, magnetic fields, and porous media, providing insights crucial for optimizing both natural and industrial processes.

PHYSICAL PROBLEM

Description of the Model

The current physical formulation aims to investigate the natural convection flow and heat transfer in a porous square enclosure filled with a non-Newtonian fluid with a constant

magnetic field. Figure 1 shows a geometrical depiction of the cavity and the coordinate system. The temperature T_h preserves the lower wall. T_c , the sidewall of the hollow is maintained cool. It is assumed that the upper wall is adiabatic. A constant magnetic field of strength B_0 is applied to the left wall. Boussinesq's approximation is used to satisfy the density in the buoyancy component, which suggests that the fluid's physical and chemical properties of the fluid and the porous media are taken for granted. Additionally, the fluid and porous media characteristics remain constant. The Darcy-Forchheimer model describes momentum transfer in porous materials.

Governing Equations

The conservation of mass, momentum, and energy is used in the following governing equations for steady two-dimensional natural convection flow in a porous cavity [26, 45].

$$\nabla \cdot \mathbf{u} = 0 \quad (1)$$

$$-\frac{1}{\rho} \frac{\partial p}{\partial x} + \frac{\nu}{1+\lambda_1} \nabla^2 \mathbf{u} - \frac{\nu}{k} \mathbf{u} = \mathbf{u} \frac{\partial \mathbf{u}}{\partial x} + \mathbf{v} \frac{\partial \mathbf{u}}{\partial y} \quad (2)$$

$$-\frac{1}{\rho} \frac{\partial p}{\partial y} + \frac{\nu}{1+\lambda_1} \nabla^2 \mathbf{v} - \frac{\sigma \beta_0^2}{\rho} \mathbf{v} + g\beta(T-T_c) - \frac{\nu}{k} \mathbf{v} = \mathbf{u} \frac{\partial \mathbf{v}}{\partial x} + \mathbf{v} \frac{\partial \mathbf{v}}{\partial y} \quad (3)$$

$$\alpha \nabla^2 T = \mathbf{u} \frac{\partial T}{\partial x} + \mathbf{v} \frac{\partial T}{\partial y} \quad (4)$$

with restricted circumstances

$$\mathbf{u}(x,0) = \mathbf{0}; \mathbf{u}(x,L) = \mathbf{0}; \mathbf{u}(0,y) = \mathbf{0}; \mathbf{u}(L,y) = \mathbf{0}; \quad (5)$$

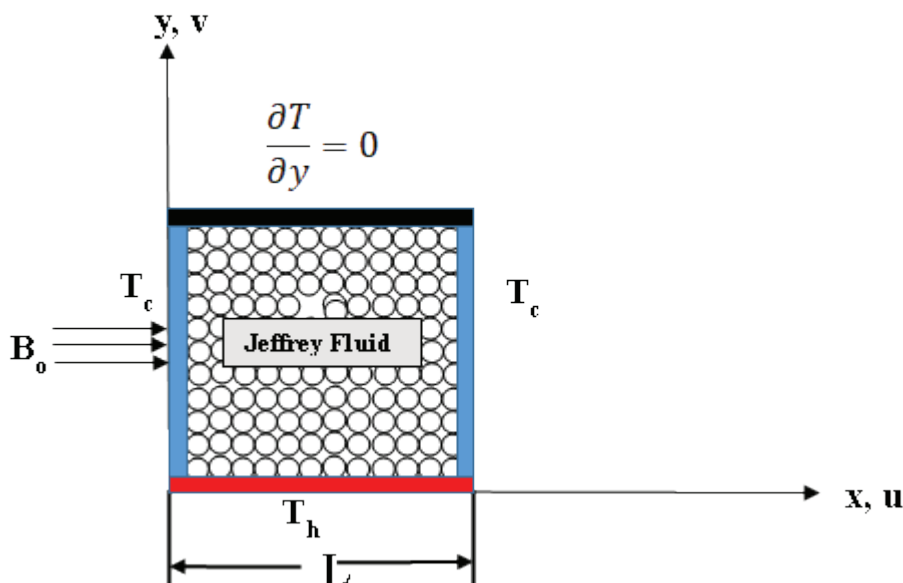


Figure 1. Schematic diagram of the physical system.

$$v(x,0) = 0; v(x,L) = 0; v(0,y) = 0; v(L,y) = 0; \quad (6)$$

$$T(x,0) = T_h; \frac{\partial T}{\partial y}(x,L) = 0; T(0,y) = T_c; T(L,y) = T_c \quad (7)$$

The following transformations can be used to obtain the dimensionless governing equations:

$$\begin{aligned} X &= \frac{x}{L}, Y = \frac{y}{L}, U = \frac{uL}{\alpha}, V = \frac{vL}{\alpha}, \theta = \frac{T-T_c}{T_h-T_c}, \\ P &= \frac{pL^2}{\rho\alpha^2}, Pr = \frac{\nu}{\alpha}, Da = \frac{K}{L^2}, \\ Ra &= \frac{g\beta(T_h-T_c)L^3Pr}{\nu^2}, Ha = \beta_0L\sqrt{\frac{\sigma}{\mu}}. \end{aligned} \quad (8)$$

The resulting dimensionless partial differential equations can be expressed as

$$\nabla \cdot U = 0 \quad (9)$$

$$-\frac{\partial P}{\partial X} + \frac{Pr}{1+\lambda_1} \nabla^2 U - \frac{Pr}{Da} U = U \frac{\partial U}{\partial X} + V \frac{\partial U}{\partial Y} \quad (10)$$

$$-\frac{\partial P}{\partial Y} + \frac{Pr}{1+\lambda_1} \nabla^2 V - Ha^2 Pr V + Ra Pr \theta - \frac{Pr}{Da} V = U \frac{\partial V}{\partial X} + V \frac{\partial V}{\partial Y} \quad (11)$$

$$\nabla^2 \theta = U \frac{\partial \theta}{\partial X} + V \frac{\partial \theta}{\partial Y} \quad (12)$$

The beginning and boundary conditions are given in nondimensional form.”

$$U(X,0) = 0; U(X,1) = 0; U(0,Y) = 0; U(1,Y) = 0; \quad (13)$$

$$V(X,0) = 0; V(X,1) = 0; V(0,Y) = 0; V(1,y) = 0; \quad (14)$$

$$\theta(X,0) = 1; \frac{\partial \theta}{\partial Y}(X,1) = 0; \theta(0,Y) = 0; \theta(1,Y) = 0. \quad (15)$$

where (u, v) represent the fluid velocity components in the (x, y) -directions, respectively. Where P is the dimensionless pressure, λ_1 is the fluid parameter, θ is the dimensionless temperature, Pr is the Prandtl number, Ra is the Rayleigh number, and Da is the Darcy number.

Nusselt Number

In heat transfer, the ratio of convective to conductive heat transfer across a fluid barrier is measured via the dimensionless Nusselt number. It is frequently used to explain forced convection and natural convection heat transfer. According to the local Nusselt number (Nu), the heat transmission coefficient is defined as

$$Nu = \pm \frac{\partial \theta}{\partial n} \quad (16)$$

where n denotes the normal direction on a plane.

The average Nusselt number is the average value of the Nusselt number over a specified region or surface. It is often employed in engineering analyses and design calculations related to heat exchangers, pipes, and other components

where heat transfer is a critical consideration. The average Nusselt numbers at the bottom are defined as

$$Nu_{avg} = \int_0^1 Nu \, dX \quad (17)$$

Problem Explanation and Mathematical Formalism

To evaluate the steady laminar, nondimensional fundamental equations 9–12 are solved with the aid of the multi-physics 6.1 software COMSOL, and the distinct boundary conditions 13–15 are resolved (Fig.2). Numerous scientific and engineering environments based on partial differential equations may be modelled and simulated via this programme. Initially, by employing the Galerkin finite element method to numerically simulate the required issue, weak formulations of nonlinear governing differential equations are generated. The finite element method discretizes large regions into smaller, more manageable units called finite elements, which are then used to solve partial differential equations.

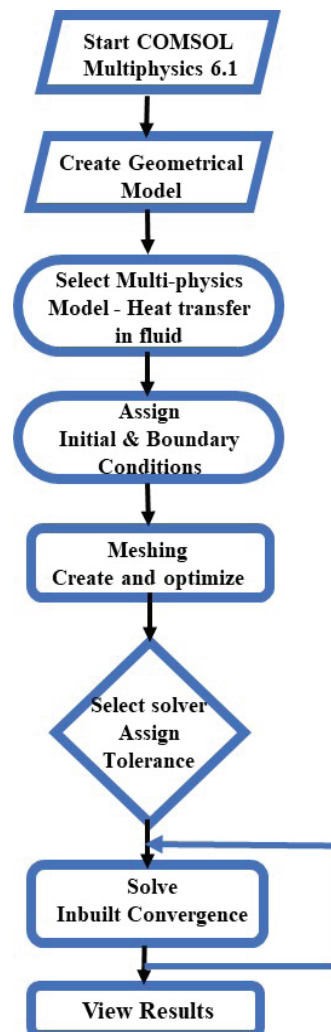


Figure 2. Flowchart for the solution procedure.

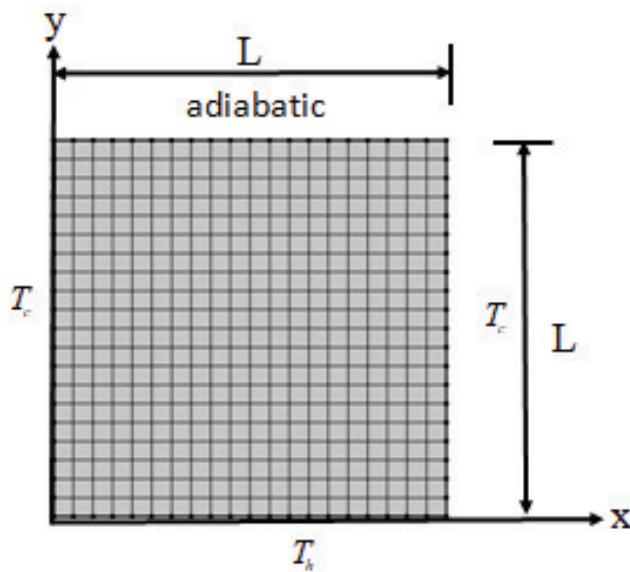


Figure 3. Optimum mesh geometry for the system configuration.

A biquadratic element is a type of finite element used in finite element methods (FEMs). It refers to a two-dimensional element where the interpolation functions (shape functions) are quadratic polynomials in both the x and y directions. The grid points (or nodes) are the discrete locations in the computational domain where the field variables are calculated. The domain consists of 20×20 biquadratic elements [46]. Since each biquadratic element spans 3 nodes in each direction, the total number of grid points can be calculated as:

$$\text{Number of grid points} = (\text{Number of elements} \times 2) + 1$$

Therefore, the computational domain consists of a 41×41 grid of points, as illustrated in Figure 3. It forms a mesh over the entire domain. These points include the nodes of the elements where calculations are performed. It provides a relatively fine resolution for the simulation, allowing for a detailed representation of the flow and thermal fields within the cavity.

Comparative Analysis and Study Validation

To verify our numerical scheme, Basak et al. [47] studied the natural convection of a Newtonian fluid in a square enclosure. The enclosure was maintained with a hot bottom wall and two cold sidewalls with an adiabatic top wall. The calculation is carried out for different Rayleigh numbers ($Ra = 10^3, 10^4, 10^5, \text{ and } 10^6$) with varying Darcy numbers ($Da = 10^{-3}, 10^{-4}, \text{ and } 10^{-5}$) for the average Nusselt number. The results for natural convection in a square porous cavity filled with Newtonian fluids have been replicated and compared with those of Basak et al. [47]. Eliminating the Jeffrey parameter leads to a Newtonian fluid, as shown in equations 10 and 11. Figure 4 depicts the obtained results and literature values, which indicate good agreement between the produced results and those of Basak et al. [47].

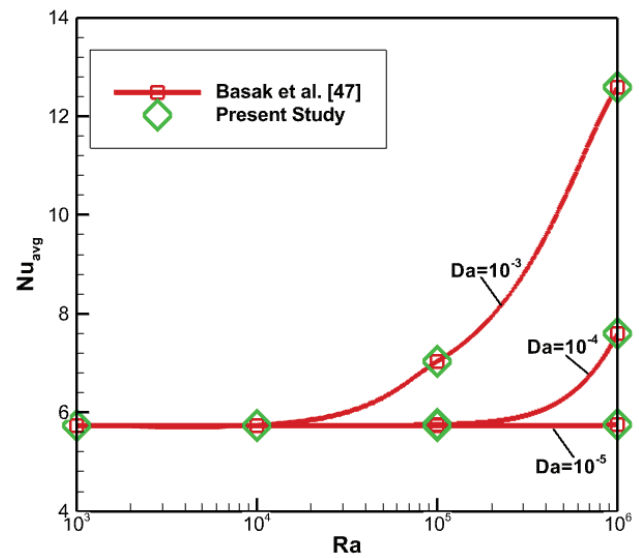


Figure 4. A comparison between the average Nusselt number at the bottom wall in the current investigation and the work of Basak et al. [47].

RESULTS AND DISCUSSION

The current work aims to analyse the steady laminar flow of natural convection heat transfer characteristics of complex fluid in a porous square cavity with a magnetic effect. This segment describes the outcomes based on the velocity distribution, Nusselt number, velocity surface, stream lines, isotherms, temperature surface, and temperature contours against different parameters, such as (λ_1), (Da), (Pr), (Ha) and (Ra). All the results are computed for fixed values of $Ra = 10^3$, $Da = 10^{-3}$, $Ha = 40$, $Pr = 10$ and $\lambda_1 = 1$.

Impact of the Velocity Distribution

The U velocity distribution with respect to the fixed Rayleigh number and Hartmann number changes, as shown in Figure 5(a), from $10 \leq Ha \leq 40$, $Ra = 10^3$, and $Da = 10^{-3}$. With respect to the increase in the u -velocity and Hartmann number, there is a symmetrical observation for the velocity distribution. Initially, the velocity in the u direction decreases to the minimum point, increases to the maximum point and then gradually decreases to 0. Point 0.5 cuts the increasing and decreasing order symmetrically. From points 0 to 0.5, the velocity decreases to the minimum point and then gradually increases. An increase in the U velocity from 0 to 0.5 indicates that the magnetic field enhances the horizontal motion of the fluid. From points 0.5 to 1, the velocity increases to the maximum point and then progressively decreases. The velocity oscillates around point 0.5. Toward the centre (approximately $x = 0.5$), the velocity becomes very small and eventually approaches zero at $x = 1$. The velocity field seems to be relatively smooth and continuous. The Hartmann number (Ha) represents the ratio of electromagnetic forces to

viscous forces in a conducting fluid. By selecting values between 10 and 40, we can observe the effects of varying electromagnetic force strengths relative to viscous forces. The chosen range allows for the observation of a symmetrical velocity distribution, which is an important aspect of the flow dynamics in the presence of a magnetic field. The symmetrical nature of the u -velocity distribution around the center ($x = 0.5$) can be clearly studied within this Hartmann number range, providing insights into how the magnetic field stabilizes the flow and reduces turbulence. The gradual suppression of horizontal motion from $x = 0.5$ to $x = 1$ at higher Hartmann numbers can be effectively analysed within this range. A decrease in the U velocity from 0.5 to 1 signifies the suppression of horizontal motion within the fluid [48]. In practical applications, such as cooling systems in nuclear reactors or electronic devices, the suppression of horizontal convection can lead to changes in heat transfer efficiency. Reduced horizontal motion might decrease the overall convective heat transfer but can increase the stability and predictability of the cooling process.

The velocity values are provided for various positions along the x -axis. The y -component of the velocity indicates the velocity of the fluid in the y -direction at each corresponding x coordinate. Figure 5(b) illustrates how the v -velocity distribution changes in relation to the fixed Hartmann and Rayleigh numbers, from $10 \leq Ha \leq 40$, $Ra = 10^3$, and $Da = 10^{-3}$. With increasing v -wave velocity, the Hartmann number decreases. The velocity profile shows variations along the x -coordinate, reaching its maximum negative value at $x = 0.5$. The velocity then starts to decrease and approaches zero toward the right end ($x = 1$). The velocity takes the wave path when the Hartmann number increases. As the Hartmann number increases, the v -velocity exhibits wave-like oscillations or paths, where the vertical motion periodically increases and then decreases, forming a characteristic wave pattern. This can occur due to the interplay of Lorentz forces, fluid inertia, and restoring forces such as pressure gradients and buoyancy.

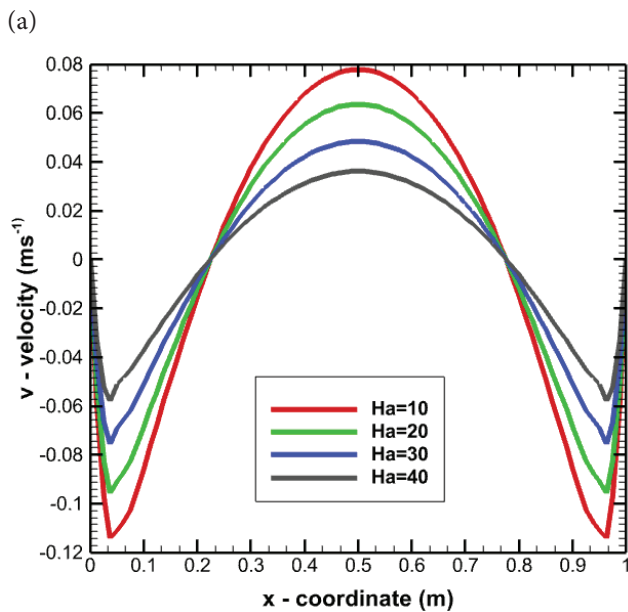
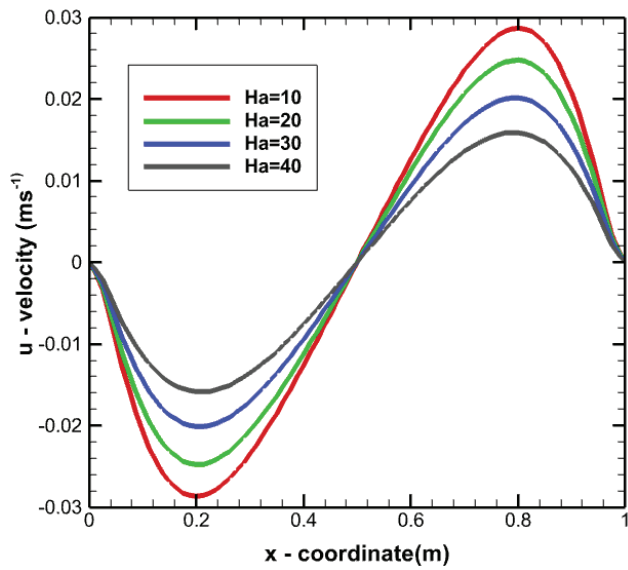
Figure 6(a) shows the velocity distribution with respect to changes in the Darcy number and fixed Hartmann number and Rayleigh number. The y -axis in the figures represents the fluid velocity in dimensionless units. The velocity is typically nondimensionalized by a characteristic velocity scale, where u varies from $10^{-3} \leq Da \leq 10^{-5}$, $Ra = 10^3$, and $Ha = 40$. In general, an increase in the Darcy number and velocity is observed as the trend decreases. However, the velocity oscillates around point 0.5. For Darcy numbers 10^{-3} , the velocity increases as x increases and gradually decreases to zero. For Darcy numbers 10^{-4} , the velocity gradually increases and then suddenly decreases when it reaches the maximum point. For Darcy numbers 10^{-5} , there is not much variation in the velocity when x increases. The velocity is constant at $y = 0$. The initial increase in horizontal velocity is due to the increased resistance to vertical flow, forcing the fluid to

channel more horizontally. A subsequent decrease in horizontal velocity occurs as the permeability becomes very low, resulting in significant resistance to flow and damping of fluid motion.

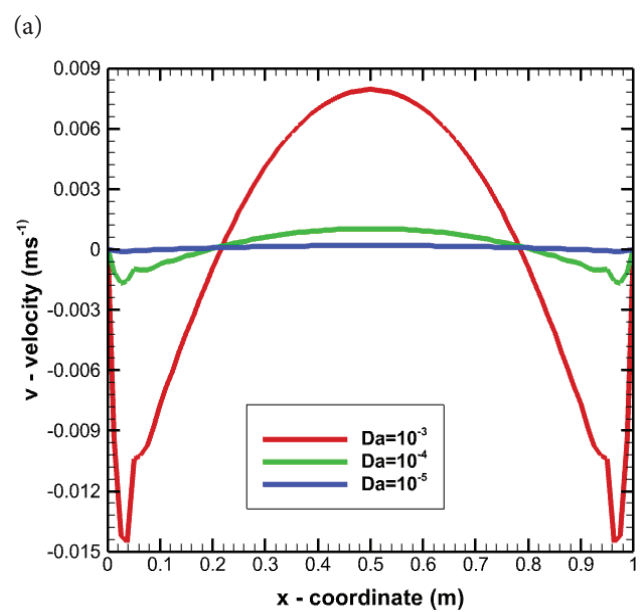
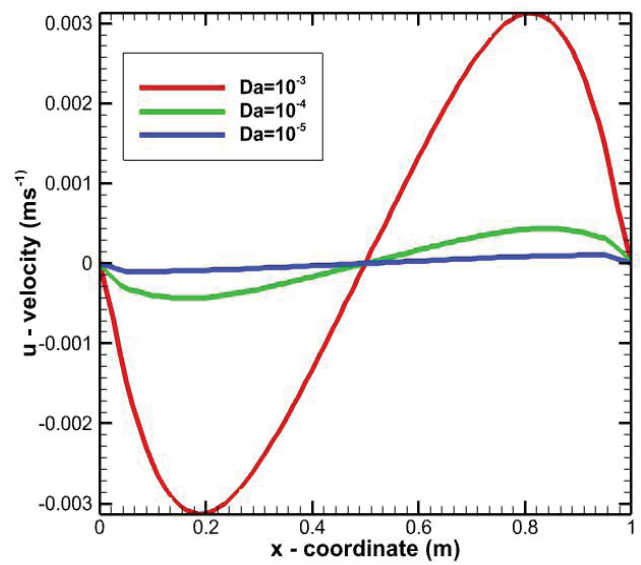
The distributions of the v -velocity with respect to variations in the Darcy number, fixed Hartmann number, and Rayleigh number are depicted in Figure 6(b). The values vary from $10^{-3} \leq Da \leq 10^{-5}$, $Ra = 10^3$, and $Ha = 40$. The y -axis shows the dimensionless vertical velocity (v). As the Darcy number decreases, indicating lower permeability, the resistance to fluid flow through the porous medium increases. This affects the vertical velocity (v). In general, with increasing Darcy integer, the velocity seems to be sinusoidal. It is symmetrical about the point 0.5. When $Da = 10^{-3}$, the velocity distribution has a long sinusoidal path. This is due to the vertical velocity as periodic instabilities and MHD waves develop due to the interaction between buoyancy forces and the increased resistance of the porous medium. For $Da = 10^{-4}$, the velocity distribution has a small sinusoidal path compared with that for $Da = 10^{-3}$, and for $Da = 10^{-5}$, the velocity distribution remains constant at the $y = 0$ point.

Figure 7(a) shows that the distributions of the u -velocity distributions with respect to a fixed Darcy number, Hartmann number and Rayleigh number differ from those for $10^3 \leq Ra \leq 10^6$, $Da = 10^{-3}$, and $Ha = 40$. The y -axis indicates the dimensionless horizontal velocity (u). The velocity field shows nonlinear behaviour, and its x -component varies significantly with spatial position. The x -component of the velocity is initially positive, peaks at approximately $x = 0.15$, then becomes negative and decreases as x increases. The velocity profile exhibits complex patterns, suggesting that intricate fluid flow behaviour is influenced by specific parameters. With increasing Rayleigh number, the velocity increases in the u direction. Higher velocities at increased Rayleigh numbers suggest enhanced mixing and more efficient heat transfer within the cavity. This is crucial for applications where rapid thermal equilibration is desired.

With respect to the fixed Hartmann number, Darcy number, and variation in the Rayleigh number, the distributions of the v -wave velocities differ for $10^3 \leq Ra \leq 10^6$, $Da = 10^{-3}$, and $Ha = 40$, and the y -axis preserves the dimensionless vertical velocity, v , as shown in Figure 7(b). The y -component of the velocity field is important and changes significantly with spatial location. With respect to the origin ($x = 0$), the velocity field is not symmetric [49]. It is shaped differently, with several peaks and troughs. At approximately $x = 0.05$, the y -component of the velocity reaches its highest negative value, whereas at approximately $x = 0.5$, it reaches its maximum positive value. The complicated fluid flow behaviour, which is impacted by particular factors, is indicated by the velocity profile. The graph indicates that the velocity along the y -axis increases with increasing Rayleigh number.



(a) (b)
Figure 5. Effect of the Hartman number on the velocity profile for $Pr = 10$, $Ra = 10^3$, and $Da = 10^{-3}$, $10 \leq Ha \leq 40$ (a) u-velocity (b) v-velocity.

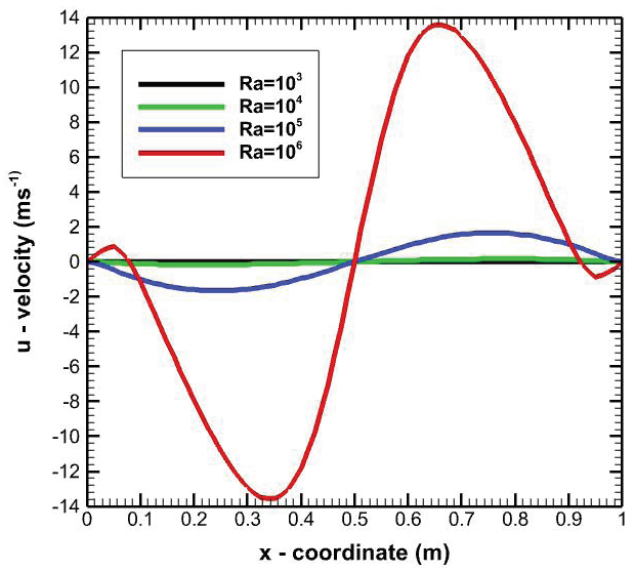


(a) (b)
Figure 6. Effect of the Darcy number on the velocity profile for $Pr = 10$, $Ra = 10^3$, $Ha = 40$, $10^{-3} \leq Da \leq 10^{-3}$ (a) u-velocity and (b) v-velocity.

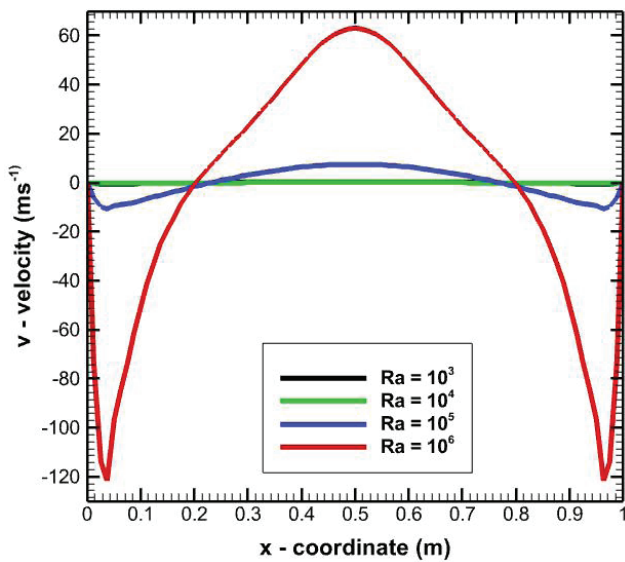
Impact of the Thermal Distribution

The Hartmann number characterizes the strength of the magnetic field in a fluid. An increase corresponds to a stronger magnetic field. In the presence of a magnetic field, particularly in the context of natural convection, magnetic forces can suppress buoyancy-driven fluid motion. Natural convection relies on density differences caused by temperature gradients to drive fluid motion. A stronger magnetic field can counteract these buoyancy forces. Figure 8(a) shows the local Nusselt number distribution for a fixed $Pr = 10$, $Ra = 10^5$, and $Da = 10^{-3}$ and the variation in the Hartmann

number fluctuates from $10 \leq Ha \leq 40$ for the hot bottom wall. The graph clearly shows that as the Hartmann number increases, the local Nusselt number decreases. Interestingly, the change in fluid behaviour occurs between points 0.3 and 0.4. The local Nusselt number tends to decrease near the sidewall of the cavity. This reveals that the interaction between the non-Newtonian characteristics of the Jeffrey fluid and the magnetic field creates a complex interplay. The rheological properties of the fluid, such as elasticity and shear-thinning, may be altered by the magnetic field, which impacts the fluid’s response to temperature gradients

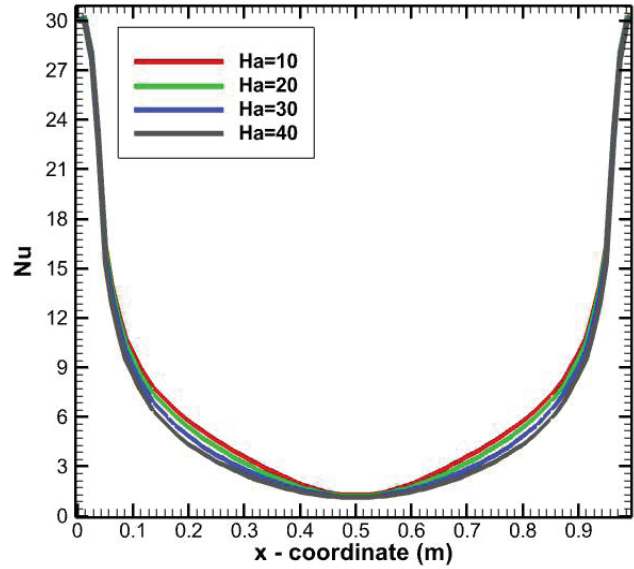


(a)

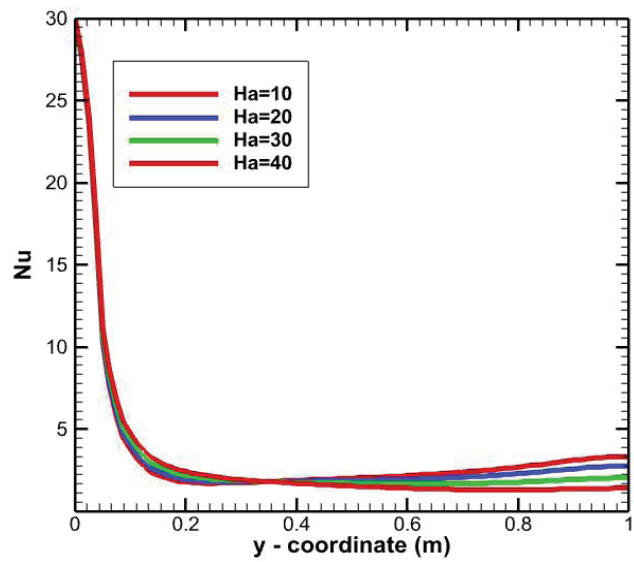


(b)

Figure 7. Effects of the Rayleigh number on the velocity profile for for $Pr = 10$, $Da = 10^{-3}$, $Ha = 40$, $10^3 \leq Ra \leq 10^6$: (a) u-velocity and (b) v-velocity.



(a)



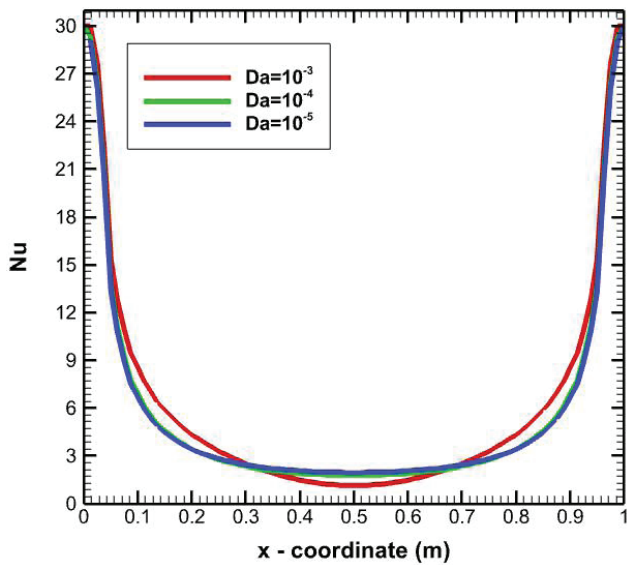
(b)

Figure 8. Effects of the Hartmann number on the local Nusselt number for $Pr = 10$, $Ra = 10^5$, $Da = 10^{-3}$, and $10 \leq Ha \leq 40$: (a) Bottom hot wall and (b) left cold wall.

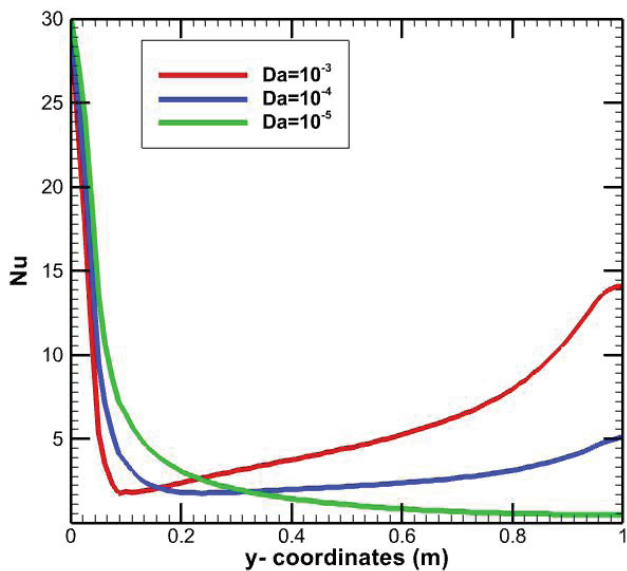
[50]. The same trend is followed for the cold wall, as shown in Figure 8(b).

A dimensionless metric called the Darcy number (Da) is used in fluid dynamics to describe how a fluid flows through a porous material. Its definition is the relationship between the fluid's dynamic viscosity and the porous medium's permeability. For a fixed Rayleigh number $Ra = 10^3$, $Pr = 10$, $Ha = 40$, and a Darcy number ranging from $10^{-3} \leq Da \leq 10^{-5}$ for the heated bottom wall of the square enclosure, Figure 9(a) shows the local Nusselt number distribution. As the Darcy number decreases, the

local Nusselt number increases. The pattern for the cold left wall shown in Figure 9(b) is a decrease in the local Nusselt number inside the cavity for every decrease in the Darcy number. The behaviour of the fluid changes at some point. For $Da = 10^{-3}$, the fluid changes its behaviour between points 0.1 and 0.2, and for $Da = 10^{-4}$, the fluid changes its behaviour around point 0.2. For $Da = 10^{-5}$, a partially smooth curve is observed from the bottom side to the top side. At certain y-coordinates, there are sharp changes in the temperature gradient, suggesting regions

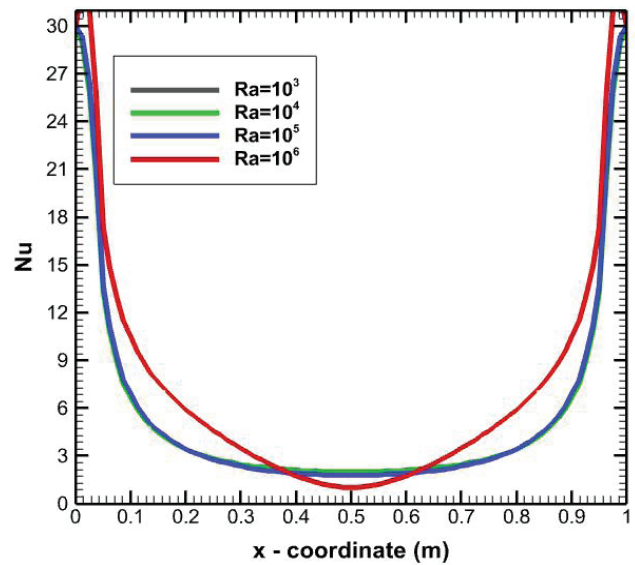


(a)

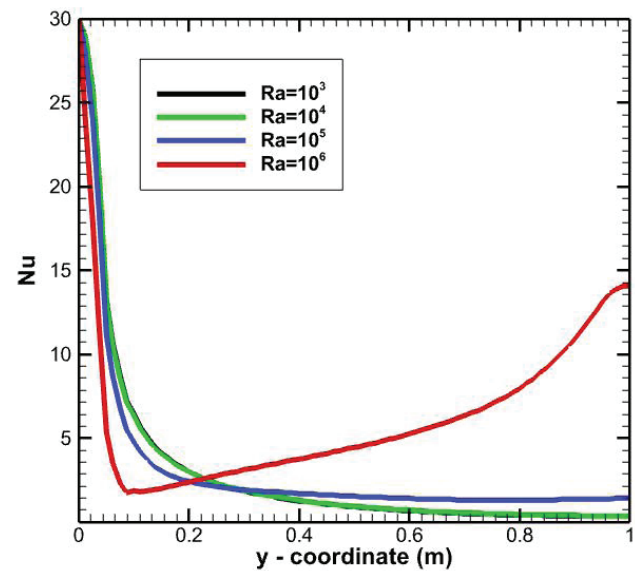


(b)

Figure 9. Effect of the Darcy number on the local Nusselt number for for $Pr = 10$, $Ra = 10^6$, $Ha = 40$ and, $10^{-3} \leq Da \leq 10^{-5}$: for the (a) bottom hot wall and (b) left cold wall.



(a)



(b)

Figure 10. Effect of the Rayleigh number on the local Nusselt number for $Pr = 10$, $Da = 10^{-3}$, $Ha = 40$, and $10^3 \leq Ra \leq 10^6$: (a) bottom hot wall and (b) left cold wall.

of intense temperature variation. The graph shows that as the Darcy number (Da) decreases, the resistance to fluid flow through the porous medium decreases. A decrease in Da could indicate more fluid motion or less flow blockage in relation to the local Nusselt number (Nu), which would alter convective heat transfer.

The relationship between the Rayleigh number and the Nusselt number is often associated with natural convection in fluid systems. The Nusselt number characterizes the convective heat transfer, and the Rayleigh number is a dimensionless parameter that represents the ratio of buoyancy to

viscosity forces. Figure 10(a) shows that the local Nusselt number distribution for a fixed $Pr = 10$, $Ha = 40$, and $Da = 10^{-3}$ varies with Rayleigh number $10^3 \leq Ra \leq 10^6$ on the bottom hot wall. An increase in the Rayleigh number corresponding to the Nusselt number decreases. Intriguingly, the difference between Raleigh numbers 10^3 , 10^4 and 10^5 is less than that of 10^6 near the sidewall. The increasing trends suggest that buoyancy has a stronger impact on heat transmission. The heated wall exhibited a similar tendency, as shown in Figure 10(b)."

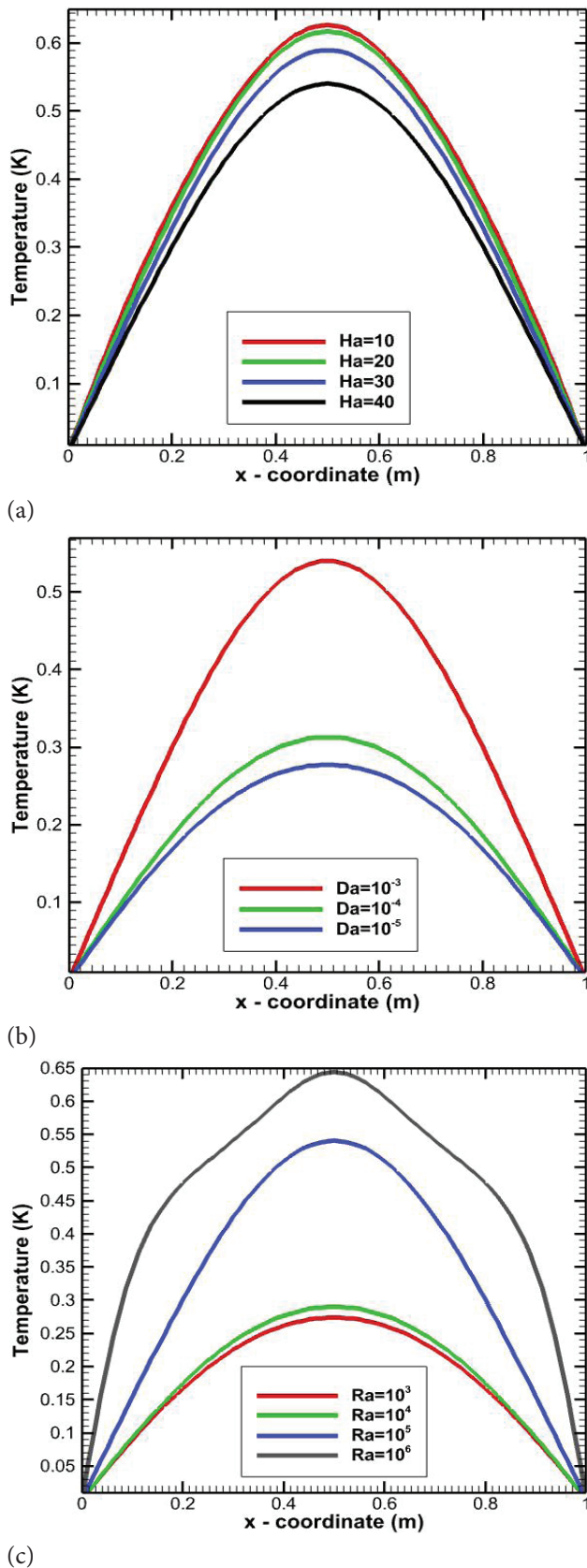


Figure 11. Effects of the Hartmann number, Rayleigh number and Darcy number on the temperature profile with a fixed $Pr = 10$: (a) $Da = 10^{-3}$, $Ra = 10^5$, $10 \leq Ha \leq 40$. (b) $Da = 10^{-3}$, $Ha = 40$, $10^3 \leq Ra \leq 10^6$ (c) $Ra = 10^5$, $Ha = 40$, $10^{-3} \leq Da \leq 10^{-5}$.

Impact of the Temperature Distribution

The temperature profile for constant parameters, such as $Pr = 10$, $Ra = 10^5$, and $Da = 10^{-3}$, is shown in Figure 11(a), and it fluctuates for Hartmann numbers of $10 \leq Ha \leq 40$. The graph unequivocally demonstrates that as the Hartmann number increases, the trend of the temperature profile decreases. This pattern indicates that a stronger magnetic field tends to reduce the velocity of the conducting fluid because of the Lorentz force. This suppression may result in a decrease in the fluid’s convective heat transfer. The y-axis shows the dimensionless temperature, θ . This nondimensionalization helps in comparing different temperature profiles irrespective of the actual temperature values, with a focus on the relative changes and distributions. The increasing influence of the magnetic field may cause changes in the flow patterns inside the hollow. This may have an effect on convective heat transfer, which might alter the distribution of temperatures. The temperature distribution becomes less steep, indicating a more uniform temperature distribution across the cavity. The stronger magnetic field dampens fluid motion, leading to more conductive rather than convective heat transfer. This concept, which is applied in biomedical devices that rely on non-Newtonian fluids, such as blood, can use magnetic fields to manage heat transfer effectively. The ability to control fluid flow and temperature distribution with varying Ha is crucial for devices such as artificial organs or thermal therapy equipment.

Figure 11(b) shows the temperature profile for fixed parameters such as $Pr = 10$, $Ha = 40$, and $Ra = 10^5$, and the Darcy number varies from $10^{-3} \leq Da \leq 10^{-5}$. The graph indicates that the trends of the temperature profile decreased with decreasing Darcy number. This is because a lower Darcy number denotes less permeability and higher resistance. The Darcy number is related to the resistance to fluid motion. This increased resistance can lead to suppressed buoyancy-driven flow within the cavity. A more gradual temperature profile is produced as the fluid motion becomes less forceful due to the decreasing dominance of buoyant forces. Convective heat transmission decreases with less fluid motion. Heat transmission to the top areas of the cavity is less effective, as the hot fluid at the bottom wall rises more slowly. The temperature distribution becomes more stratified as a result of this restriction on convective heat transfer. Consequently, a lower Darcy number results in a more gradual temperature profile within the cavity by reducing permeability, inhibiting buoyancy-driven flow, limiting convective heat transfer, and enhancing thermal stratification. In nuclear reactors, heat transfer management is crucial for both safety and performance. A lower Darcy number can aid in limiting convective heat transfer, minimizing hotspots and ensuring a more uniform temperature distribution in the reactor core. This decrease in heat transmission can improve the stability and safety of nuclear reactors, allowing for more accurate control over reactor parameters.

Figure 11(c) shows the temperature profiles for fixed parameters such as $Pr = 10$, $Ha = 40$, and $Da = 10^{-3}$, for Rayleigh numbers of $10^3 \leq Ra \leq 10^6$. Notably, the increasing Rayleigh number of the temperature profile also tends to increase. This pattern shows that buoyancy-driven convection causes fluid circulation in response to temperature changes within the cavity. As Ra increases, the differences in temperature between the hot and cold limits become more apparent. The warmer fluid close to the heated surface rises, whereas the colder fluid at the cold surface decreases. Increased buoyancy-driven flow, enhanced convective heat transfer, and increased thermal mixing caused by an increase in the Rayleigh number all contribute to increased temperatures. Solar collectors and geothermal energy systems frequently use non-Newtonian fluids to improve thermal performance. The capacity to detect and improve natural convection inside the system increases the overall energy conversion efficiency. The findings of

temperature profiles with variable Ra values can help in the design of more efficient energy systems, ensuring effective heat extraction or dissipation.

Velocity Surface, Stream Line, Temperature Surface, and Isotherm Contour

Figure 12 shows the velocity surface for $Pr = 10$, $Ra = 10^6$, $Da = 10^{-3}$, and $10 \leq Ha \leq 40$. Heat transfer is observed for increased Hartmann numbers. The bottom walls of the closed surface were heated. The fluid behaviour in the bottom wall changes with increasing Hartmann number. As the Hartmann number (Ha) increases, there is a noticeable suppression of velocity within the cavity. This suppression occurs because the magnetic field exerts a Lorentz force that opposes fluid motion, particularly in the horizontal direction. The resulting velocity profile becomes more uniform at higher Ha , indicating stronger magnetic damping effects.

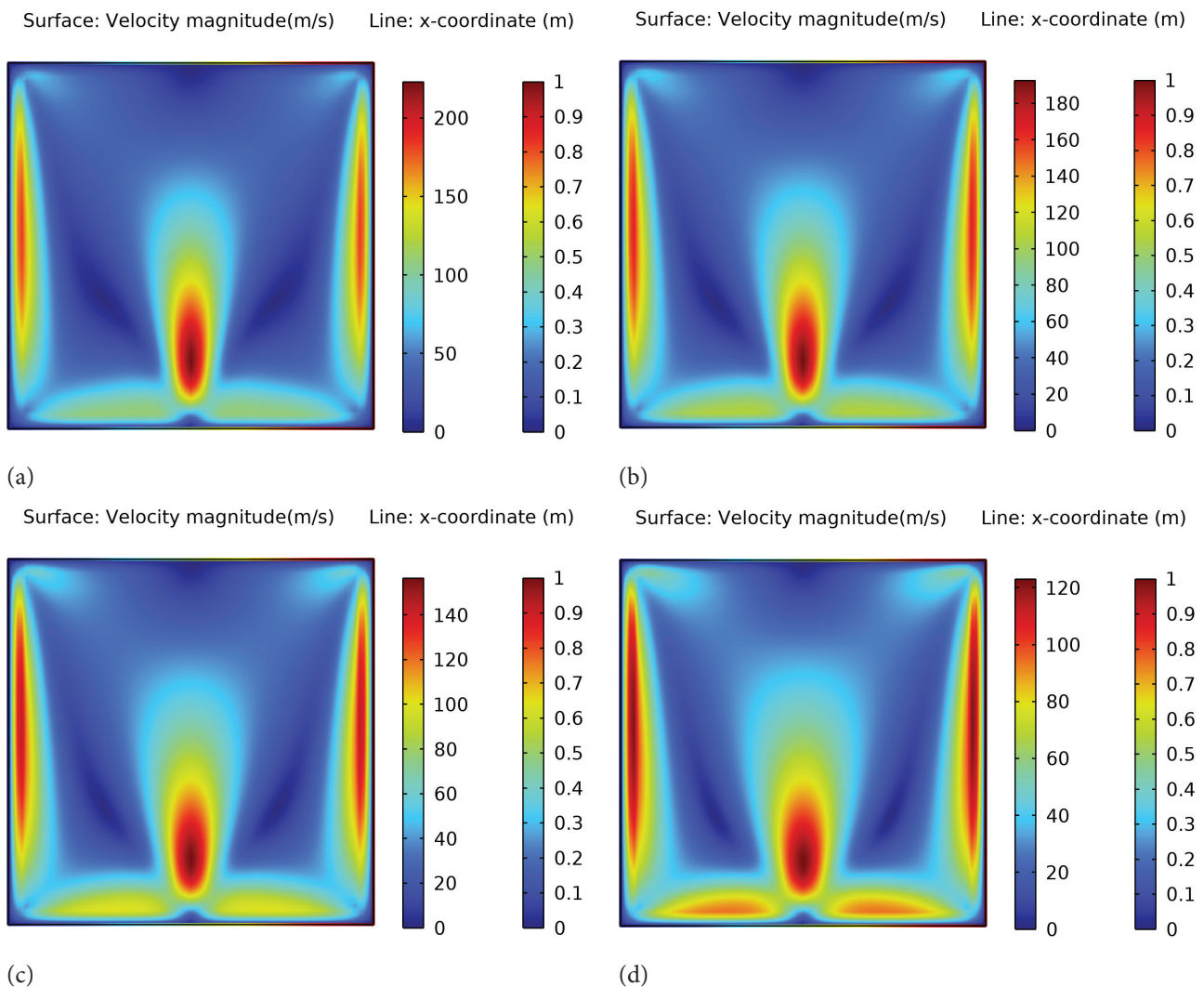


Figure 12. (a,b,c,d) Velocity surface for $Pr = 10$, $Da = 10^{-3}$, $Ra = 10^6$, $10 \leq Ha \leq 40$.

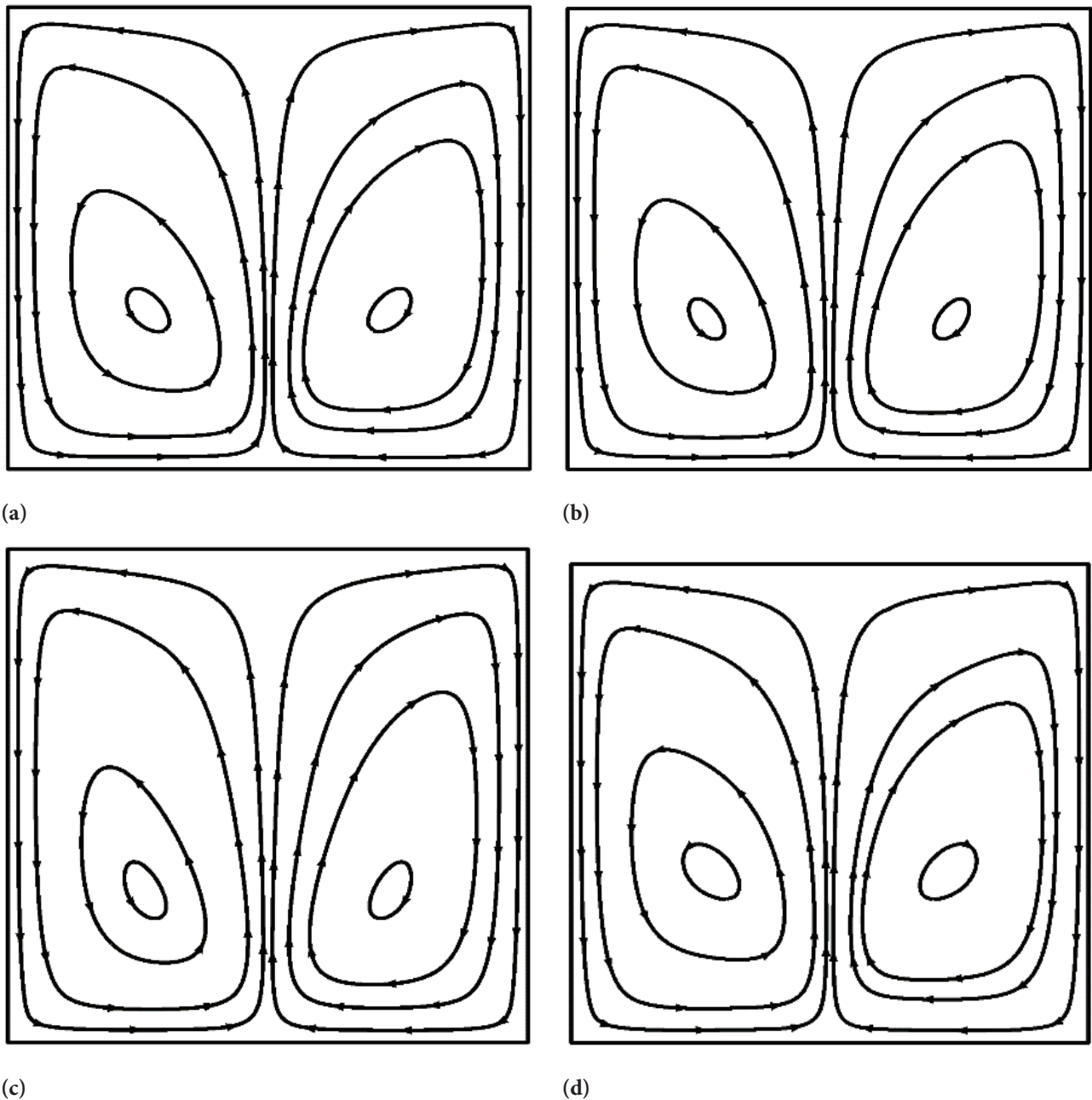


Figure 13. (a,b,c,d) Stream line for $Pr = 10$, $Da = 10^{-3}$, $Ra = 10^6$, $10 \leq Ha \leq 40$.

The streamlines of the velocity for $Pr = 10$, $Ra = 10^6$, $Da = 10^{-3}$, and $10 \leq Ha \leq 40$ are shown in Figure 13. A horizontal magnetic field is applied. The streamlines reveal that at lower Ha , the fluid motion is more vigorous, with pronounced circulation cells forming due to buoyancy forces. There is evidence of both clockwise and anticlockwise circulation development. The circulation split into two rollers that were vertical. The direction of circulation is anticlockwise near the right wall and clockwise near the left wall. As the Hartmann number increases, the fluid

rises from the bottom wall's center to its highest point. After that, it flows smoothly to the side to create a vertical roll. The temperature contours are concentrated towards the sidewall and bottom wall margins as a result of the enhanced circulation, which may result in a higher convective heat transfer rate.

Figure 14 shows the surface temperatures for $Pr = 10$, $Ra = 10^6$, $Da = 10^{-3}$, and $10 \leq Ha \leq 40$. As the Hartmann number increased, the trend increased. The fluid flow increases from the bottom and from the middle part, and the fluid

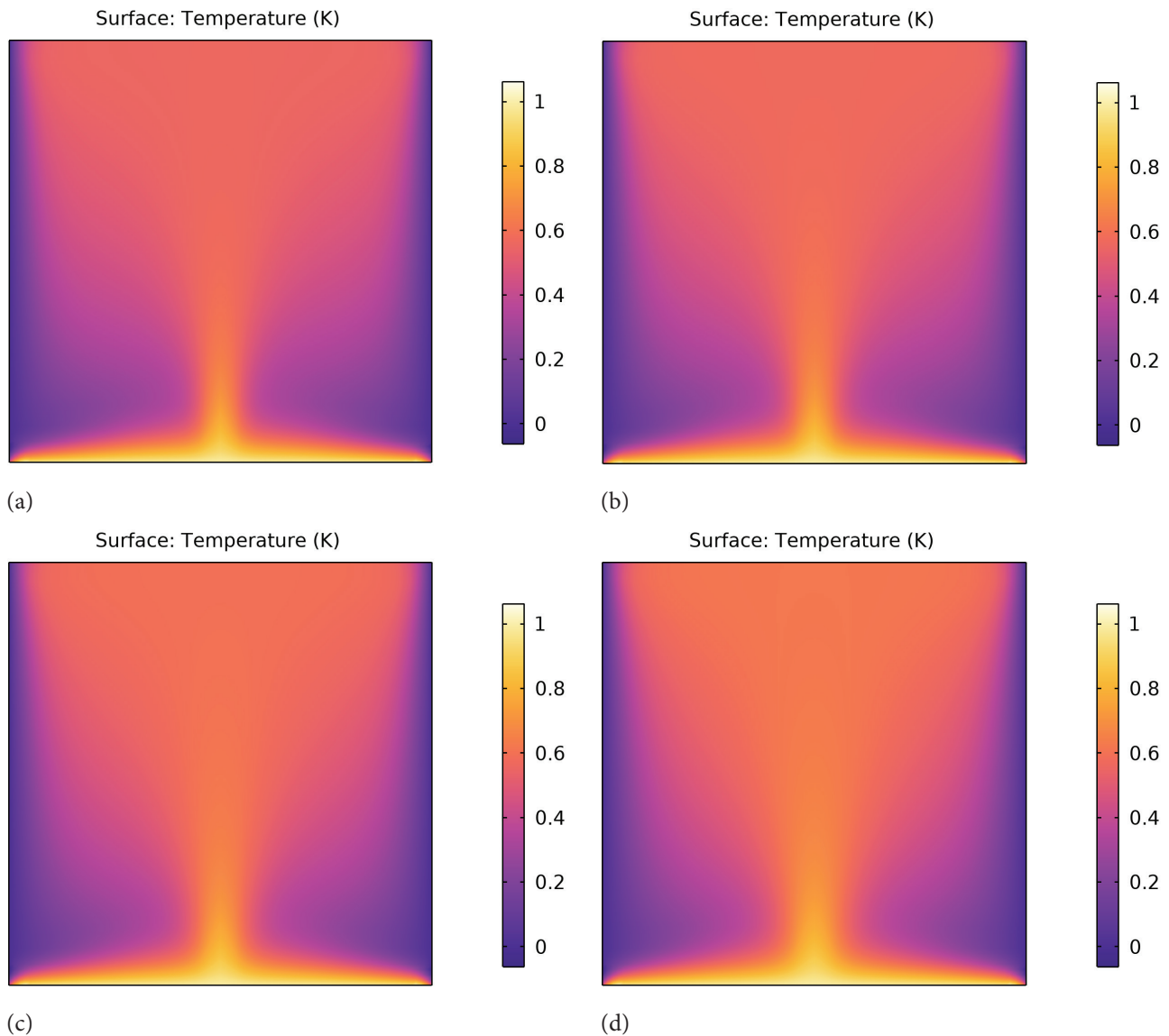


Figure 14.(a,b,c,d) Temperature surface for $Pr = 10$, $Da = 10^{-3}$, $Ra = 10^6$, $10 \leq Ha \leq 40$.

spreads to the side and top wall. With increasing Hartmann number, the thickness of the fluid flow increases. At lower Ha , the temperature surface shows significant thermal gradients, corresponding to active convective heat transfer. As Ha increases, these gradients diminish, indicating that convection is being suppressed and conduction becomes more dominant, leading to a more uniform temperature distribution.

The temperature contours for $Pr = 10$, $Ra = 10^6$, $Da = 10^{-3}$, and $10 \leq Ha \leq 40$ are displayed in Figure 15. Remarkably, eddies within the square cavity are found to exhibit an increase in the Hartmann number. Few eddies developed at the top of the cavity's two corners at $Ha = 10$. Few eddies form inside the larger eddies at the cavity's upper two corners for $Ha = 20$. Furthermore, eddies that

formed at the top walls of the two corners, $Ha = 30$ and 40 , likewise rose. The formation of multiple eddies can impact heat transfer within the cavity. Smaller, localized eddies can enhance mixing and thus improve heat transfer efficiency in certain regions while potentially reducing it in others because of the dampening effect of the magnetic field. The contours are closely spaced at lower Ha , showing strong convective heat transfer with steep temperature gradients.

The isotherm surfaces for $Pr = 10$, $Ra = 10^6$, $Da = 10^{-3}$, and $10 \leq Ha \leq 40$ are displayed in Figure 16. The isotherm decreases as the magnetic field increases, and heat is transferred from the bottom of the porous medium to its top surface. These findings indicate that increasing the magnetohydrodynamic effect decreases the isotherm effect.

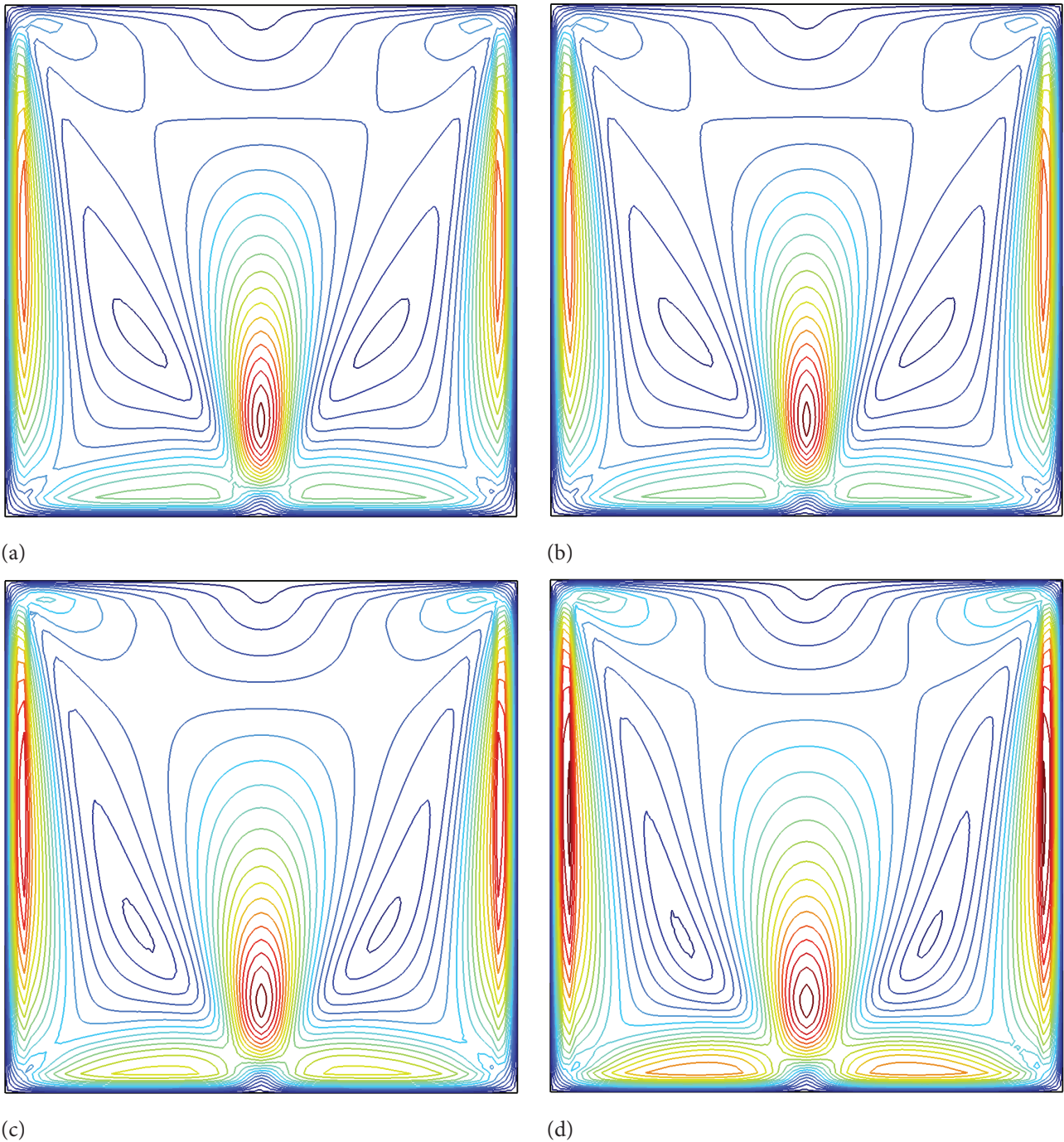


Figure 15. (a,b,c,d) Temperature contour for $Pr = 10$, $Ra = 10^6$, $Da = 10^{-3}$, $10 \leq Ha \leq 40$.

Figure 17 shows the contour lines of isotherms for $Pr = 10$, $Ra = 10^6$, $Da = 10^{-3}$, and $10 \leq Ha \leq 40$. An increase in the Hartmann number decreases in the contour lines. That is, for a higher Hartmann number, the contour line occupies the cavity. From the analysis, it is clear that with a lower Ra , the isotherms suggest a reduced convective activity, with more conduction-dominated heat transfer. The presence of a magnetic field further stabilizes the temperature

distribution, smoothing out the isotherms, particularly at higher Ha values.

Average Nusselt Number

The average Nusselt number, a dimensionless metric, is used to quantify the effectiveness of convective heat transmission in a fluid. It is common to describe the ratio of conductive to convective heat transfer. The Nusselt number is the ratio of conductive heat transmission to convective heat

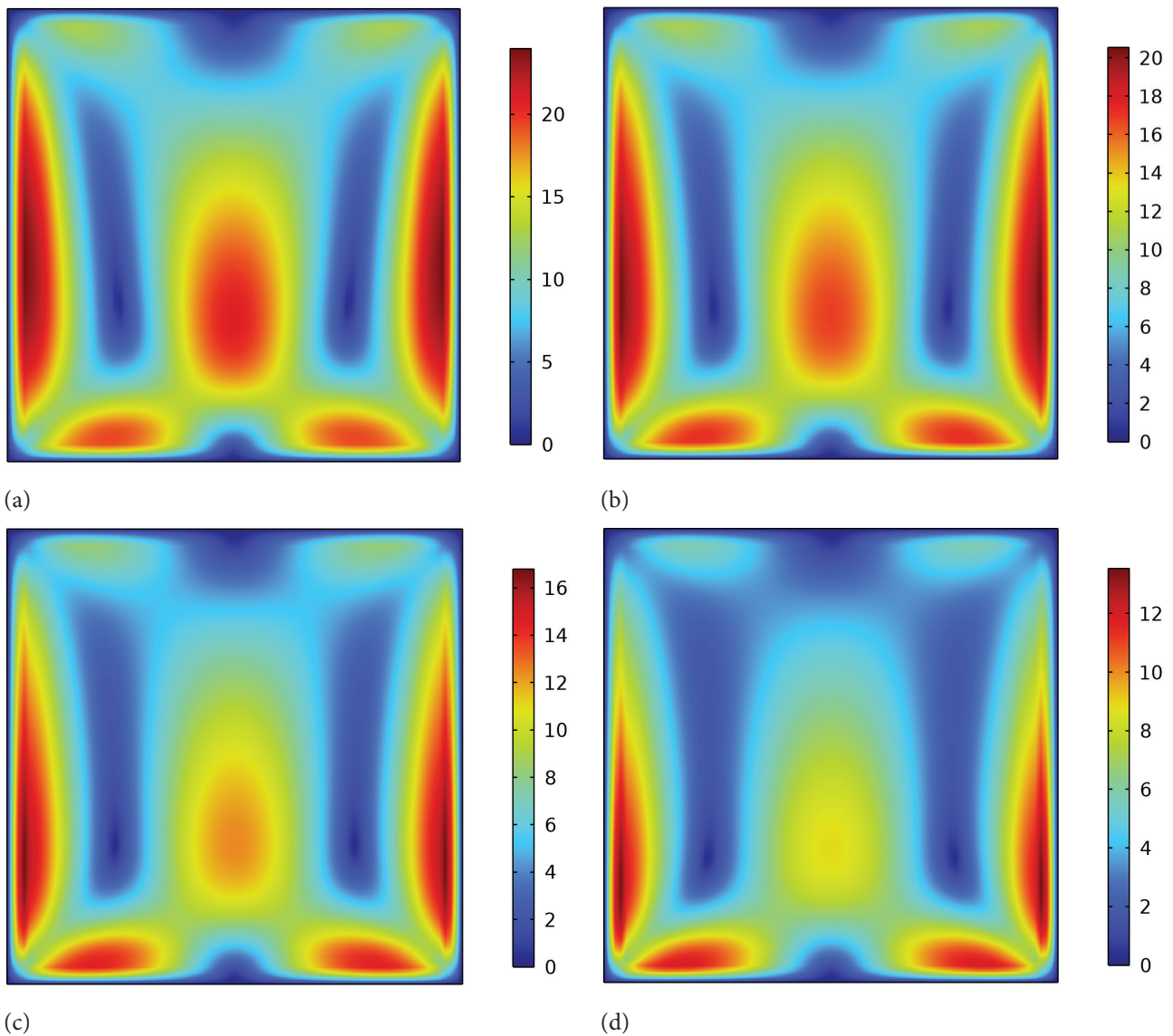


Figure 16. (a,b,c,d) Isotherm surface for $Pr = 10$, $Da = 10^{-3}$, $Ra = 10^5$, $10 \leq Ha \leq 40$.

transfer over a boundary layer. The average Nusselt number is the mean value across the whole surface. With respect to the Rayleigh number, Darcy number and Hartmann number, Table 1 shows the average Nusselt number. The Rayleigh and Hartmann numbers and the average Nusselt number had a negative relationship. It is difficult to enable efficient convective heat transmission when the mean Nusselt number decreases in conjunction with increasing Rayleigh and Hartmann numbers. One reason for this could be that convective currents are not as powerful as magnetic field effects. Furthermore, Table 2 shows the relationships between the Rayleigh number and the Hartmann number, Darcy number and average Nusselt number in cold wall cavities. The table illustrates the complex interplay between magnetic field effects, buoyancy-driven convection, and

conductive heat transfer. The results indicate a change in the prevailing regime in favour of a magnetic effect-dominated regime that amplifies the influence of conductive heat transfer processes while decreasing convective heat transfer. While combining the effect, at low Ra (10^3), the Nusselt number remains almost constant across different Ha and Da , indicating that convection is weak, and heat transfer is primarily by conduction. At higher Ra (10^6), significant variations in Nu are observed, demonstrating that convection becomes dominant, but is increasingly modulated by the magnetic field (Ha) and the porous medium (Da). These findings are critical for applications where controlling thermal transport is crucial, such as in cooling systems or geological formations where fluid flow occurs through porous materials.

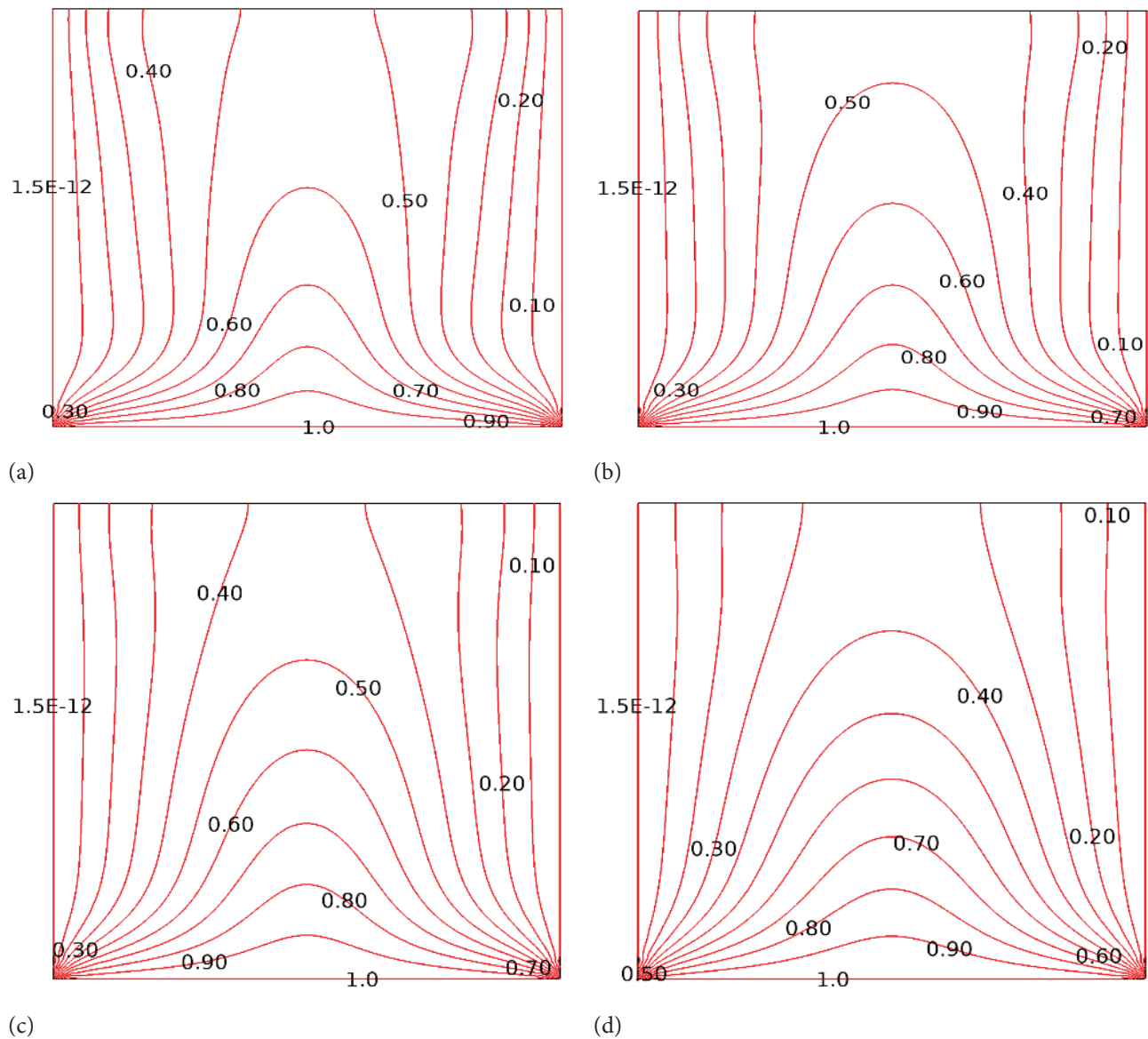


Figure 17. (a,b,c,d). Isotherm Contour for $Pr = 10$, $Da = 10^{-3}$, $Ra = 10^5$, $10 \leq Ha \leq 40$.

Table 1. Effects of the Hartmann number, Rayleigh number and Darcy number on the average Nusselt number for the bottom (hot) wall

		Rayleigh number			
		$Ra = 10^3$	$Ra = 10^4$	$Ra = 10^5$	$Ra = 10^6$
Hartmann number	$Ha = 10$	5.72857	5.74285	7.15135	13.64529
	$Ha = 20$	5.72849	5.73983	6.86564	13.34419
	$Ha = 30$	5.72840	5.73694	6.52641	12.90466
	$Ha = 40$	5.72832	5.73479	6.23704	12.38008
Darcy number	$Da = 10^{-3}$	5.72832	5.73479	6.23704	12.38008
	$Da = 10^{-4}$	5.72797	5.72908	5.74968	7.43254
	$Da = 10^{-5}$	5.72784	5.72766	5.72604	5.72456
	$Da = 10^{-6}$	5.72780	5.72729	5.72220	5.67105

Table 2. Effects of the Hartmann number, Rayleigh number and Darcy number on the average Nusselt number for the left (cold) wall

		Rayleigh number			
		$Ra = 10^3$	$Ra = 10^4$	$Ra = 10^5$	$Ra = 10^6$
Hartmann number	$Ha = 10$	2.863931	2.8639	3.51644	6.95268
	$Ha = 20$	2.86398	2.86336	3.37372	6.78630
	$Ha = 30$	2.86404	2.86298	3.20705	6.54320
	$Ha = 40$	2.86410	2.86292	3.06870	6.25312
Darcy number	$Da = 10^{-3}$	2.86410	2.86292	3.06870	6.25313
	$Da = 10^{-4}$	2.86432	2.86420	2.86770	3.69930
	$Da = 10^{-5}$	2.86441	2.86502	2.87109	2.93773
	$Da = 10^{-6}$	2.86440	2.86488	2.86967	2.91806

CONCLUSION

In a square cavity filled with a permeability matrix, the primary goal of the current work is to investigate the impact of MHD on Jeffrey fluid flow under natural convection flow. The complex, nonlinear mathematical equations that control the Jeffrey fluid are very detailed. Therefore, to provide a numerical solution, one may often utilize the COMSOL Multiphysics 6.1 approach. The Nusselt number, velocity surface, stream lines, isotherms, temperature surface, and temperature contours were all solved via the Galerkin finite element method. Non-Newtonian fluids are useful when modelling the movement of magma in volcanic cavities or other geological structures. Jeffrey fluids provide a more accurate picture of the complex rheological behaviour of molten rock. When mixing polymers or other materials in chemical processes, the behavior of non-Newtonian fluids in cavities is crucial. Jeffrey fluids allow a better understanding and simulation of the component distribution and mixing efficiency in such processes. These findings provide valuable insights for a broader audience interested in the application of MHD and non-Newtonian fluid dynamics in geological and industrial processes. Understanding the intricate behavior of Jeffrey fluids under varying magnetic fields and permeable conditions can lead to better predictions and optimizations in relevant applications, such as magma flow modelling and polymer processing. The findings of the current analysis are as follows:

1. The increase and subsequent decrease in the U-wave velocity with increasing Hartmann number reflect the complex interplay between the magnetic field strength and fluid dynamics. At lower Hartmann numbers, horizontal flow is enhanced, whereas at higher Hartmann numbers, the damping effects of the magnetic field dominate, reducing the horizontal velocity.
2. An initial increase in vertical velocity occurs because of constrained vertical pathways that focus on fluid motion. The formation of sinusoidal patterns in the vertical velocity as periodic instabilities and MHD

waves develop is due to the interaction between buoyancy forces and the increased resistance of the porous medium.

3. The initial increase in horizontal velocity is due to the increased resistance to vertical flow, forcing the fluid to channel more horizontally. A subsequent decrease in horizontal velocity occurs as the permeability becomes very low, resulting in significant resistance to flow and damping of fluid motion.
4. An initial increase in vertical velocity occurs because of constrained vertical pathways that focus on fluid motion. The formation of sinusoidal patterns in the vertical velocity as periodic instabilities and MHD waves develop is due to the interaction between buoyancy forces and the increased resistance of the porous medium.
5. At higher Rayleigh numbers, convective heat transfer is dominant, leading to higher average Nusselt numbers. However, this is modulated by both the strength of the magnetic field and the permeability of the porous medium.

NOMENCLATURE

u, v	Velocity component of x,y direction (ms^{-1})
U, V	Dimensionless velocity component
x, y	Cartesian coordinates (m)
X, Y	Dimensionless Cartesian coordinates
p	Pressure (Nm^{-2})
P	Dimensionless Pressure
Pr	Prandlt number
Da	Darcy number
Ra	Rayleigh number
T	Temperature (K)
T_h	Temperature of hot bottom wall (K)
T_c	Temperature of vertical cold wall (K)
Nu	Nusselt number
Nu_{avg}	Average Nusselt number
L	Side of the square cavity (m)
K	Porosity of the material (m^2)

Greek symbols

B	Coefficient of thermal expansion (k^{-1})
α	Thermal diffusivity (m^2s^{-1})
θ	Dimensionless Temperature
ρ	Density of fluid (kgm^{-3})
λ_1	Jeffrey fluid parameter
σ	Electrical conductivity (Sm^{-1})
ν	Kinematic Viscosity (m^2s^{-1})
μ	Dynamic Viscosity (Nms^{-1})

AUTHORSHIP CONTRIBUTIONS

Authors equally contributed to this work.

DATA AVAILABILITY STATEMENT

The authors confirm that the data that supports the findings of this study are available within the article. Raw data that support the finding of this study are available from the corresponding author, upon reasonable request.

CONFLICT OF INTEREST

The authors declared no potential conflicts of interest with respect to the research, authorship, and/or publication of this article.

ETHICS

There are no ethical issues with the publication of this manuscript.

REFERENCES

- [1] Mullick SH, Kumar A, Kundu PK. Numerical study of natural convection inside a square cavity with non-uniform heating from top. *J Inst Eng (India) Ser C* 2020;101:1043–1050.[\[CrossRef\]](#)
- [2] Selimefendigil F, Senol G, Öztop HF, Abu-Hamdeh NH. A review on non-Newtonian nanofluid applications for convection in cavities under magnetic field. *Symmetry* 2023;15:41.[\[CrossRef\]](#)
- [3] Hamid M, Usman M, Khan ZH, Haq RU, Wang W. Heat transfer and flow analysis of Casson fluid in a partially heated trapezoidal cavity. *Int Commun Heat Mass Transf* 2019;108:104284.[\[CrossRef\]](#)
- [4] Anthony AS, Verma TN. Numerical analysis of natural convection in a heated room and its implication on thermal comfort. *J Therm Eng* 2021;7:37–53.[\[CrossRef\]](#)
- [5] Hussien AA, Al-Kouz W, El Hassan M, Janvekar AA, Chamkha AJ. A review of flow and heat transfer in cavities and their applications. *Eur Phys J Plus* 2021;136:353.[\[CrossRef\]](#)
- [6] Babu DH, Tarakaramu N, Narayana PVS, Sarojamma G, Makinde OD. MHD flow and heat transfer of a Jeffrey fluid over a porous stretching/shrinking sheet with a convective boundary condition. *Int J Heat Technol* 2021;39:885–894.[\[CrossRef\]](#)
- [7] Makkar V, Poply V, Goyal R, Sharma N. Numerical investigation of MHD Casson nanofluid flow towards a nonlinear stretching sheet in the presence of double-diffusive effects along with viscous and Ohmic dissipation. *J Therm Eng* 2021;7:1–17.[\[CrossRef\]](#)
- [8] Prasad A, Rajkumar S, Teklemariam A, Tafesse D, Tufa M, Bejaxhin BH. Influence of nano additives on performance and emissions characteristics of a diesel engine fueled with watermelon methyl ester. *J Therm Eng* 2023;9:395–400.[\[CrossRef\]](#)
- [9] Basiri M, Goshayeshi H, Chaer I, Pourpasha H, Heris SZ. Experimental study on heat transfer from rectangular fins in combined convection. *J Therm Eng* 2023;9:1632–1642.[\[CrossRef\]](#)
- [10] Mohammed AA. Natural convection heat transfer inside horizontal circular enclosure with triangular cylinder at different angles of inclination. *J Therm Eng* 2021;7:240–254.[\[CrossRef\]](#)
- [11] Zhu L, He X, Wu X, Wu J, Hong T. Recent development of abrasive machining processes enhanced with non-Newtonian fluids. *Coatings* 2024;14:779.[\[CrossRef\]](#)
- [12] Aman S, Al-Mdallal Q, Khan I. Heat transfer and second order slip effect on MHD flow of fractional Maxwell fluid in a porous medium. *J King Saud Univ Sci* 2018;32:450–458.[\[CrossRef\]](#)
- [13] Shkarah AJ. Convective heat transfer and fully developed flow for circular tube Newtonian and non-Newtonian fluids condition. *J Therm Eng* 2021;7:409–414.[\[CrossRef\]](#)
- [14] Anusha T, Mahabaleshwar US, Bhattacharyya S. An impact of MHD and radiation on flow of Jeffrey fluid with carbon nanotubes over a stretching/shrinking sheet with Navier’s slip. *J Therm Anal Calorim* 2023;148:12597–12607.[\[CrossRef\]](#)
- [15] Siddique I, Adrees R, Ahmad H, Askar S. MHD free convection flows of Jeffrey fluid with Prabhakar-like fractional model subject to generalized thermal transport. *Sci Rep* 2023;13:9289.[\[CrossRef\]](#)
- [16] Raisi A. Natural convection of non-Newtonian fluids in a square cavity with a localized heat source. *J Mech Eng* 2016;62:553–564.[\[CrossRef\]](#)
- [17] Dimitrienko YI, Shuguang L. Numerical simulation of MHD natural convection heat transfer in a square cavity filled with Carreau fluids under magnetic fields in different directions. *Comp Appl Math* 2020;39:1–26.[\[CrossRef\]](#)
- [18] Liao CC, Li WK, Chu CC. Analysis of heat transfer transition of thermally driven flow within a square enclosure under effects of inclined magnetic field. *Int Comm Heat Mass Transf* 2022;130:105817.[\[CrossRef\]](#)
- [19] Sajjadi H, Amiri Delouei A, Sheikholeslami M, Atashafrooz M. Double MRT Lattice Boltzmann simulation of 3-D MHD natural convection in a cubic cavity with sinusoidal temperature distribution utilizing nanofluid. *Int J Heat Mass Transf* 2018;126:489–503.[\[CrossRef\]](#)

- [20] Miroshnichenko V, Sheremet MA, Oztop HF, Abu-Hamdeh N. Natural convection of $\text{Al}_2\text{O}_3/\text{H}_2\text{O}$ nanofluid in an open inclined cavity with a heat-generating element. *Int J Heat Mass Transf* 2018;126:184–191.[\[CrossRef\]](#)
- [21] VahabzadehBozorg M, Siavashi M. Two-phase mixed convection heat transfer and entropy generation analysis of a non-Newtonian nanofluid inside a cavity with internal rotating heater and cooler. *Int J Mech Sci* 2019;151:842–857.[\[CrossRef\]](#)
- [22] Abu-Nada E, Pop I, Mahian O. A dissipative particle dynamics two-component nanofluid heat transfer model: Application to natural convection. *Int J Heat Mass Transf* 2019;133:1086–1098.[\[CrossRef\]](#)
- [23] Keyhani-Asl A, Hossainpour S, Rashidi MM, Sheremet MA, Yang Z. Comprehensive investigation of solid and porous fins' influence on natural convection in an inclined rectangular enclosure. *Int J Heat Mass Transf* 2019;133:729–744.[\[CrossRef\]](#)
- [24] Sajjadi H, Amiri Delouei A, Sheikholeslami M, Atashafrooz M. Simulation of three-dimensional MHD natural convection using double MRT Lattice Boltzmann method. *Physica A Stat Mech Appl* 2019;515:474–496.[\[CrossRef\]](#)
- [25] Pekmen Geridönmez B. Numerical simulation of natural convection in a porous cavity filled with ferrofluid in presence of magnetic source. *J Therm Eng* 2018;4:1756–1769.[\[CrossRef\]](#)
- [26] Aneja M, Chandra A, Sharma S. Natural convection in a partially heated porous cavity to Casson fluid. *Int Comm Heat Mass Transf* 2020;114:104555.[\[CrossRef\]](#)
- [27] Horimek A. Non-Newtonian natural-convection cooling of a heat source of variable length and position placed at the bottom of a square cavity. *Therm Sci* 2023;27:4161–4178.[\[CrossRef\]](#)
- [28] Raje A, Ashlesha AB, Kulkarni A. Entropy analysis of the MHD Jeffrey fluid flow in an inclined porous pipe with convective boundaries. *Int J Thermofluids* 2023;17:100275.[\[CrossRef\]](#)
- [29] Li Y, Wang Y, Pang L, Xiao L, Ding Z, Duan P. Research progress of plasma/MHD flow control in inlet. *Chin J Theor Appl Mech* 2019;51:311–321.
- [30] Karimi MS, Oboodi MJ. Investigation and recent developments in aerodynamic heating and drag reduction for hypersonic flows. *Heat Mass Transf* 2019;55:547–569.[\[CrossRef\]](#)
- [31] Nazee M, Ali N, Javed T, Nazir MW. Numerical analysis of the full MHD model with the Galerkin finite-element method. *Eur Phys J Plus* 2019;134:204.[\[CrossRef\]](#)
- [32] Mwapinga A, Mureithi E, Makungu J, Masanja V. MHD arterial blood flow and mass transfer under the presence of stenosis, body acceleration and chemical reaction: a case of magnetic therapy. *J Math Informatics* 2020;18:85–103.[\[CrossRef\]](#)
- [33] Dharmiah G, Rama Prasad JL, Balamurugan KS, Nurhidayat I, Fernandez-Gamiz U, Noeiaghdam S. Performance of magnetic dipole contribution on ferromagnetic non-Newtonian radiative MHD blood flow: an application of biotechnology and medical sciences. *Heliyon* 2023;9:e13369.[\[CrossRef\]](#)
- [34] Chen X, Zhao L, Wang F, Peng A. Numerical analysis of the self-propulsion performance of seawater MHD propulsion underwater vehicle. *Magneto hydrodynamics* 2023;59:7.[\[CrossRef\]](#)
- [35] Selvi RK, Muthuraj R. MHD oscillatory flow of a Jeffrey fluid in a vertical porous channel with viscous dissipation. *Ain Shams Eng J* 2018;9:2503–2516.[\[CrossRef\]](#)
- [36] Sarada K, Gowda RJP, Sarris IE, Kumar RN, Prasannakumara BC. Effect of magneto hydrodynamics on heat transfer behaviour of a non-Newtonian fluid flow over a stretching sheet under local thermal non-equilibrium condition. *Fluids* 2021;6:264.[\[CrossRef\]](#)
- [37] Shaheen S, Bég OA, Gul F, Maqbool K. Electro-osmotic propulsion of Jeffrey fluid in a ciliated channel under the effect of nonlinear radiation and heat source/sink. *J Biomech Eng* 2021;143:051008.[\[CrossRef\]](#)
- [38] Ahmed SY, Al-Amir QR, Hamzah HK, Ali FH, Abed AM, Al-Manea AA, et al. Investigation of natural convection and entropy generation of non-Newtonian flow in molten polymer-filled odd-shaped cavities using finite difference lattice Boltzmann method. *Numer Heat Transf Part B Fundam* 2024;1–26.[\[CrossRef\]](#)
- [39] Yasmeen S, Asghar S, Anjum HJ, Ehsan T. Analysis of Hartmann boundary layer peristaltic flow of Jeffrey fluid: Quantitative and qualitative approaches. *Comm Nonlinear Sci Numer Simul* 2019;76:51–65.[\[CrossRef\]](#)
- [40] Ali A, Maqsood M, Anjum HJ, Awais M, Sulaiman M. Analysis of heat transfer on MHD Jeffrey nanofluid flow over nonlinear elongating surface of variable thickness. *J Appl Math Mech* 2021;102:e202100250.[\[CrossRef\]](#)
- [41] Reddappa B, Parandhama A, Venkateswara Raju K, Sreenadh S. Analysis of the boundary layer flow of thermally conducting Jeffrey fluid over a stratified exponentially stretching sheet. *Turk J Comput Math Educ* 2021;12:730–739.
- [42] Ishtiaq F, Ellahi R, Bhatti MM, Alamri SZ. Insight in thermally radiative cilia-driven flow of electrically conducting non-Newtonian Jeffrey fluid under the influence of induced magnetic field. *Mathematics* 2022;10:2007.[\[CrossRef\]](#)
- [43] Reddappa B, SudheerBabu M, Sreenadh S. Magneto hydrodynamic (MHD) Jeffrey nanofluid flow over an exponentially stretching sheet through a porous medium. *AIP Conf Proc* 2023;2649:030003.[\[CrossRef\]](#)

- [44] Khan A, Gul T, Ali I, Abd El-Wahed HK, Taseer M, Alghamdi W, et al. Thermal examination for double diffusive MHD Jeffrey fluid flow through the space of disc and cone apparatus subject to impact of multiple rotations. *Int J Heat Fluid Flow* 2024;106:109295. [\[CrossRef\]](#)
- [45] Yadav D. Effect of electric field on the onset of Jeffrey fluid convection in a heat-generating porous medium layer. *Pramana J Phys* 2022;96:23. [\[CrossRef\]](#)
- [46] Basak T, Roy S. Natural convection in a square cavity filled with a porous medium: effects of various thermal boundary conditions. *Int J Heat Mass Transf* 2006;49:1430–1441. [\[CrossRef\]](#)
- [47] Basak T, Roy S, Balakrishnan AR. Effects of thermal boundary conditions on natural convection flows within a square cavity. *Int J Heat Mass Transf* 2006;49:4525–4535. [\[CrossRef\]](#)
- [48] Khan ZH, Khan WA, Hamid M. Non-Newtonian fluid flow around a Y-shaped fin embedded in a square cavity. *J Therm Anal Calorim* 2021;143:573–585. [\[CrossRef\]](#)
- [49] Nield DA, Bejan A. *Convection in Porous Media*. 3rd ed. New York: Springer; 2006.
- [50] Dimitrienko YI, Li S. Numerical simulation of MHD natural convection heat transfer in a square cavity filled with Carreau fluids under magnetic fields in different directions. *Comput Appl Math* 2020;39:252. [\[CrossRef\]](#)